OUKA
Osaka University Knowledge Archive

Title	High-resolution multislice X-ray ptychography of extended thick objects
Author(s)	Suzuki, Akihiro; Furutaku, Shin; Shimomura, Kei et al.
Citation	Physical Review Letters. 2014, 112(5), p. 053903
Version Type	VoR
URL	https://hdl.handle.net/11094/86935
rights	Copyright 2014 by the American Physical Society
Note	

Osaka University Knowledge Archive : OUKA

https://ir.library.osaka-u.ac.jp/

Osaka University

High-Resolution Multislice X-Ray Ptychography of Extended Thick Objects

Akihiro Suzuki,[1] Shin Furutaku,[1] Kei Shimomura,[1] Kazuto Yamauchi,[1] Yoshiki Kohmura,[2] Tetsuya Ishikawa,[2] and Yukio Takahashi[1,*]

[1]*Graduate School of Engineering, Osaka University, 2-1 Yamada-oka, Suita, Osaka 565-0871, Japan*
[2]*RIKEN SPring-8 Center, 1-1-1 Kouto, Sayo-cho, Sayo, Hyogo 679-5148, Japan*
(Received 12 August 2013; revised manuscript received 11 November 2013; published 4 February 2014)

We report the first demonstration of hard x-ray ptychography using a multislice approach, which can solve the problem of the limited spatial resolution under the projection approximation. We measured ptychographic diffraction patterns of a two-layered object with a 105 μm gap using 7 keV focused coherent x rays. We successfully reconstructed the phase map of each layer at ∼50 nm resolution using a multislice approach, while the resolution was worse than ∼192 nm under the projection approximation. The present method has the potential to enable the three-dimensional high-resolution observation of extended thick specimens in materials science and biology.

DOI: 10.1103/PhysRevLett.112.053903 PACS numbers: 42.25.Fx, 42.25.Kb, 42.30.Rx

Ptychography is a method that was proposed in the 1960s [1] as a means of solving the phase problem and was first demonstrated in 1970 [2]. Ptychography is regarded as a coherent diffractive imaging method (CDI) [3] that enables the observation of a sample at a high-spatial resolution without a lens, in which the diffraction pattern is measured at a far field and is then directly phased to obtain an image. The original concept of CDI employed a plane-wave geometry [4], in which the sample is illuminated with a plane wave. Plane-wave CDI has a significant limitation; that is, the sample must be an isolated object. Ptychography was the breakthrough that overcame this limitation, in which a probe is scanned across the sample and the diffraction pattern is observed at each beam position, allowing the observation of extended objects. Since its initial demonstration, ptychography using x rays has been demonstrated [5] and applied to the observation of biological samples in two [6] and three dimensions [7], the quantitative imaging of strains [8,9] and dislocations [10], and the local imaging of magnetic moments [11] and ferroelectric polarization [12] in thin films, chemical imaging using the absorption edge [13–15], the characterization of wave fields in focusing x rays [16–19], and the analysis of mixed states [20]. X-ray ptychography is one of the most promising CDI methods for use in biology, materials science, and optics.

A significant advantage of x-ray ptychography is that it provides high-resolution images of extended thick objects because of the short wavelength and high-penetration power of x rays. The spatial resolution of CDI is limited, in principle, by only the x-ray wavelength and the largest scattering angle that can be recorded, i.e., highest-Q diffraction. It is known that the diffraction intensity rapidly decays with increasing magnitude of the scattering vector. Highly focused hard x-ray beams are useful for collecting high-Q diffraction data with a high signal-to-noise ratio. Focused x-ray ptychography has provided high-resolution projection images of thin objects at sub-20 nm resolution [21–23]. In addition to the intensity issue, the "projection approximation" [24], which is implicit in CDI, is the other important factor of limiting the spatial resolution in x-ray ptychography. The projection approximation treats the properties of a 3D diffracting structure via an integral along the optical axis, which is justified when the object is thinner than the depth of focus. As the resolution approaches the wavelength, the thickness effect of objects plays a significant role in CDI and causes the breakdown of the projection approximation [25], which means that the projection approximation limits the maximum thickness of the object for a desired spatial resolution. In plane-wave CDI, a few approaches without the projection approximation, such as precession measurement [26] and ankylography [27], can be employed under certain conditions, while such approaches have not yet been developed for x-ray ptychography. A new approach is therefore required to enable the high-resolution x-ray ptychography of thick objects.

A multislice approach [28] is a method that can be used to overcome the limited spatial resolution resulting from applying the projection approximation to thick objects. In this method, the exit surface wave of an illuminated object is calculated and the projection method is applied in a slice-by-slice manner. Recently, ptychography using a multislice approach has been demonstrated in a visible-light experiment [29], in which the small focal depth of the visible light, i.e., the significant difference between probe functions through the slices, enabled an effective ptychographic reconstruction. In addition, the difficulty in applying the multislice approach to x-ray experiments has been pointed out since the difference between the multislice approximation and the exit surface wave obtained under the projection approximation is small [30].

 © 2014 American Physical Society

In this Letter, we report the first demonstration of focused x-ray ptychography using the multislice approach. We obtain projection images with a spatial resolution beyond the limitation under the projection approximation and discuss how to generalize the approach to unknown samples.

Our experiment on multislice x-ray ptychography was carried out at BL29XUL [31] in SPring-8. Figure 1(a) shows a schematic of the experimental setup. x and y are the horizontal and vertical axes, respectively, and z is the axis parallel to the beam propagation direction. A 7.000 keV monochromatic x-ray beam (wavelength $\lambda = 0.1771$ nm) was generated by an in-vacuum undulator device and a Si(111) double-crystal monochromator. The monochromatic x-ray beam was two-dimensionally focused to a ~500 nm spot size using Kirkpatrick-Baez mirror optics. The flux of the focused x rays was estimated to be $\sim 1 \times 10^8$ photons/s. The test sample was a two-layered nanostructured object with a 105 μm gap between the layers. A 50-nm-thick Pt film was deposited on two 500-nm-thick SiN membrane chips, and the two chips were pasted together with a 105 μm gap between them. The gap was produced using particles with a mean particle size of 100 ± 5 μm (Sekisui Chemical Co., Ltd: Micropeal GS) and its width was determined using an optical microscope. Patterns comprising the characters of "SACLA" and "SPring8" were fabricated on the Pt film on the membrane in the upstream and downstream regions, respectively, using a FIB. Figure 1(b) shows field-emission scanning electron microscopy (FE-SEM) images of each pattern. The phase shift of the 50-nm-thick Pt film at 7.000 keV was estimated to be ~0.123 rad, which justifies the use of the weak phase object approximation. The test sample was positioned at the focal plane. The focal depth of the mirror was ~6 mm, which was approximately 60 times longer than the gap width between the two layers in the sample. Coherent forward diffraction patterns were recorded with an x-ray direct-detection CCD. The x-ray exposure time at each position was 20 s. It took ~7.5 h to collect the 112 ptychographic diffraction patterns in an 8×14 overlapping field, which includes the readout time from the CCD.

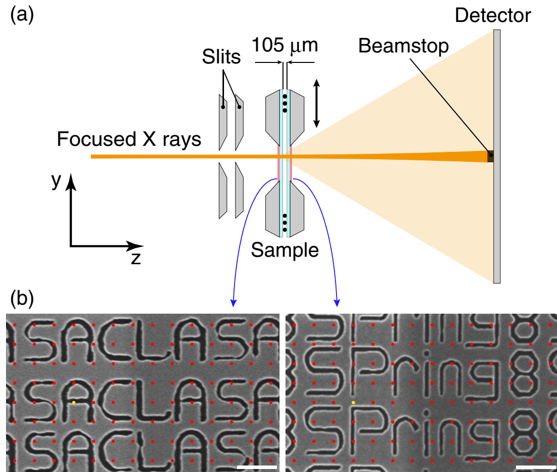

FIG. 1 (color online). (a) Schematic of the multislice x-ray ptychography experiment. X rays of 7 keV were two-dimensionally focused to a ~500 nm spot size using Kirkpatrick-Baez mirrors. The sample was composed of two layers with a 105 μm gap between them and patterns comprising the characters of "SACLA" and "SPring8" fabricated on them. The SACLA pattern was located at the focal plane. Forward diffraction intensities were collected using a CCD detector with a pixel size of 20×20 μm^2, which was positioned at a distance of 1368 mm from the focal point. A beamstop of size $\sim 650 \times 650$ μm^2 was placed in front of the CCD. The sample was illuminated in 8×14 overlapping fields of view that were separated by 500 nm in the horizontal and vertical directions. (b) FE-SEM images of the two patterns. The SEM image of SACLA is laterally inverted. The scale bar is 1 μm. The dots indicate the centers of the focused x-ray beam in the scan.

Figure 2(a) shows the coherent diffraction pattern in the region -25 μm$^{-1} \leq q_x \leq 25$ μm^{-1} and -25 μm$^{-1} \leq q_y \leq 25$ μm^{-1} when the focused x rays were irradiated at the light-colored dot in Fig. 1(b). The maximum values of q_x and q_y that satisfy the projection approximation for the sample thickness D_z are expressed as [32]

$$q_{x,\max}^{\text{projection}} = q_{y,\max}^{\text{projection}} \approx \frac{1}{\sqrt{2D_z\lambda}}, \tag{1}$$

where λ is the x ray wavelength. In the present experiment ($D_z = 105$ μm, $\lambda = 0.1771$ nm), $q_{x,\max}^{\text{projection}}$ and $q_{y,\max}^{\text{projection}}$ are ~ 5.2 μm^{-1}. The achievable spatial resolution in the x and y directions under the projection approximation is estimated to be ~192 nm ($= 1/q_{x,\max}^{\text{projection}} = 1/q_{y,\max}^{\text{projection}}$), corresponding to the size of two pixels in the projection image reconstructed from the diffraction pattern in the region -5.2 μm$^{-1} \leq q_x \leq 5.2$ μm^{-1} and -5.2 μm$^{-1} \leq q_y \leq 5.2$ μm^{-1}.

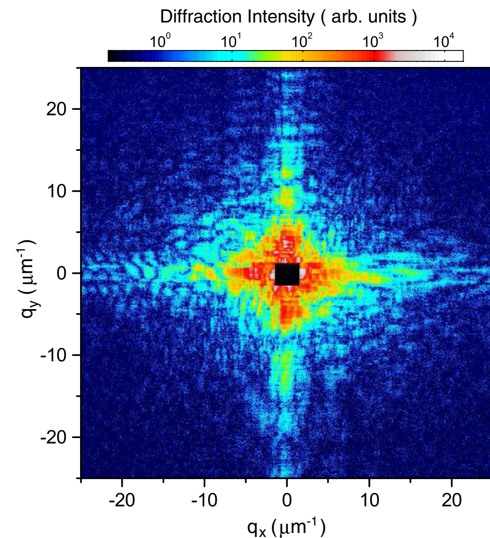

FIG. 2 (color online). Coherent diffraction pattern of the test object observed at the position indicated by a light-colored dot in Fig. 1(b). $\boldsymbol{q}$ is defined as $|\boldsymbol{q}| = 2\sin(\Theta/2)/\lambda$, where Θ is the scattering angle and λ is the x ray wavelength. The diffraction pattern is composed of an array of 606×606 pixels.

Next, we reconstructed the complex transmission function of the sample from the 112 diffraction patterns in $-25\,\mu\text{m}^{-1} \leq q_x \leq 25\,\mu\text{m}^{-1}$ and $-25\,\mu\text{m}^{-1} \leq q_y \leq 25\,\mu\text{m}^{-1}$ using the extended ptychographical iterative engine (ePIE) [33] and multislice ePIE [29] (3PIE) within the weak phase object approximation [34]. A test chart (NTT-AT:ATN/XRESO-50) was measured beforehand in the present setup. The derived illumination wave field was used as the initial illumination function for the reconstruction of the two-layered object. The reconstruction of the object started from two flat objects of unit transmission separated by 105 μm. The width of the gap and the number of slices were fixed in the iteration process. The wave propagation between the slices was calculated by the angular spectrum method [35]. During the first 20 iterations, the illumination function was not updated. After that, the object and illumination functions were updated. The iterative process was continued for up to 2×10^3 iterations. To evaluate the convergence of each reconstruction, the normalized error in the diffraction patterns was calculated after each iteration, which is defined as [33]

$$E_\Psi = \frac{\sum_j \sum_q |\sqrt{I_j(q_x, q_y)} - |\Psi_j(q_x, q_y)||^2}{\sum_j \sum_q I_j(q_x, q_y)}, \qquad (2)$$

where j is the number of consecutive recorded diffraction patterns, I is the diffraction intensity, and Ψ is the retrieved wave front in the diffraction plane.

Figures 3(a) and 3(b) show the phase maps obtained in the upstream and downstream slices, respectively, reconstructed using 3PIE. The projection of the two patterns SACLA and SPring8 is clearly visualized. The phase shift at each pattern is ~0.12 rad, which is in good agreement with the theoretical value. Figure 3(c) shows the phase map produced by superimposing the images in Figs. 3(a) and 3(b). Figure 3(d) shows the phase map of the test sample reconstructed using ePIE. The resolution of the image in Fig. 3(d) is worse than that in Fig. 3(c). Moreover, numerous artifacts appeared in the image in Fig. 3(d). Figure 3(e) plots the evolution of the error over 2×10^3 iterations of the two algorithms. After 1×10^3 iterations, the error has hardly changed in each plot. The error of 3PIE is ~0.05 smaller than that of ePIE. It is evident that 3PIE provides a more precise image than ePIE.

Next, we evaluated the spatial resolution of the phase maps reconstructed using 3PIE. Figure 4(a) shows an enlarged view of the area indicated by the square in Figs. 3(a) and 3(b) and an FE-SEM image of the same area. Structural defects due to the instability of the FIB nanomachining are included in the test pattern, which are shown by arrows in Fig. 3(a). Our reconstruction agrees well with the FE-SEM image, which indicates the high-spatial resolution of the images reconstructed using 3PIE. Figure 4(b) shows line profiles through P and Q in Fig. 4(a). The FWHM was determined to be 52.0 ± 1.2 nm for P and 53.0 ± 2.1 nm for Q. The spatial resolution along

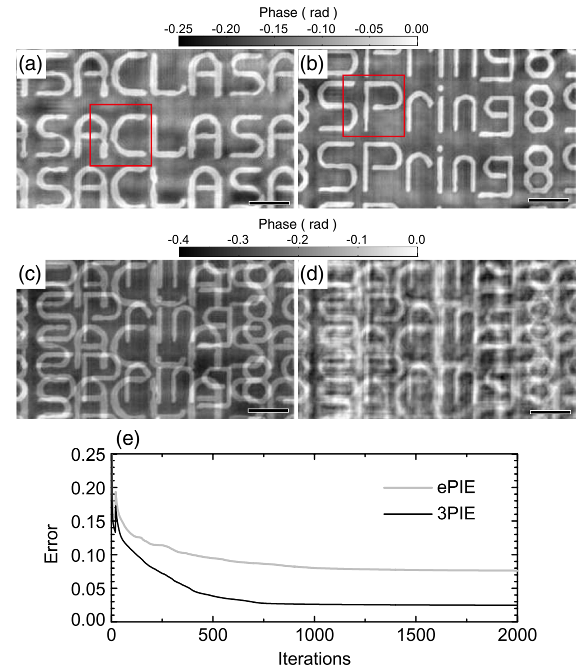

FIG. 3 (color online). (a)–(d) Phase maps of the test sample reconstructed using (a)–(c) 3PIE and (d) ePIE. (a),(b) Images reconstructed in the first and second slices, respectively. (c) Projection produced by superimposing (a) and (b). The pixel size is 20.0 nm. The total number of pixels is 200×350. The scale bar is 1 μm. (e) Evolution of the error metric E_Ψ during the ePIE and 3PIE reconstructions.

the x and y directions is much better than the limitation value under the projection approximation. On the other hand, although an accurate value of the spatial resolution along the z direction cannot be determined from only the present result, it should be better than 105 μm because the

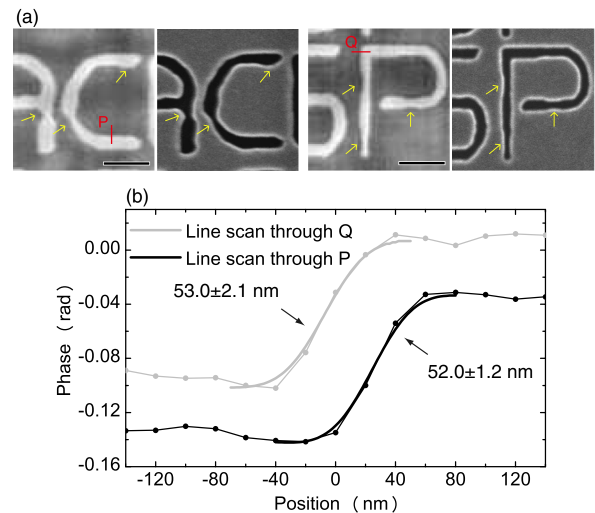

FIG. 4 (color online). (a) (left) Enlarged view of the area indicated by a square in Figs. 3(a) and 3(b) and (right) FE-SEM image of the same area. The scale bar is 500 nm. (b) Line profiles through P and Q in (a) and FWHM for each profile. The line scan through Q is shifted by 0.05 rad.

two-layered object with a 105 μm gap was separately reconstructed. In addition, we can theoretically consider the spatial resolution as follows. Multislice x-ray ptychography reconstructs a 3D image from coherent diffraction patterns recorded at single incident angles. The basic concept is similar to that of anklyography [27]; i.e., 3D information of the object is extracted from the diffraction patterns on a curved Ewald surface. The spatial resolution of multislice x-ray ptychography can therefore be described similarly to that ankylography [27], which is determined as [32]

$$d_x = d_y = \frac{\lambda}{\sin(\Theta_{\max})}, \qquad d_z = \frac{\lambda}{2\sin^2(\Theta_{\max}/2)}, \quad (3)$$

where d_x, d_y, and d_z represent the resolution along the x, y, and z directions, respectively. $\Theta_{\max}$ is the maximum scattering angle in the observed diffraction pattern. According to this formula, the achievable spatial resolution in the present experiment is estimated to be 40 nm for d_x and d_y and 18 μm for d_z. The d_x and d_y values are close to the experimental values. The slight difference between the theoretical and experimental values is due to the statistical error of the high-Q diffraction intensities and/or the sharpness of the object itself. On the other hand, the d_z value is much smaller than the width of the gap between the two layers, which is consistent with the result of 3PIE reconstructions with various gaps [32].

To understand why multislice ptychography worked well in the x-ray experiment, we compared the illumination wave field in the first and second slices. Figures 5(a) and 5(b), respectively, show intensity maps of the reconstructed illumination wave field in the first and second slices when the focused x rays were irradiated at the light-colored dot in Fig. 1(b). The intensity distribution in the first slice is a good agreement with that in the second slice since the focal depth is much longer than the gap width. Figure 5(c) shows the difference between the intensities in the second slice with and without the sample, corresponding to the hologram pattern due to the interference between the scattered x rays from the upstream sample and the penetrating x rays. Figures 5(d) and 5(e) show phase maps of the reconstructed illumination wave field in the first and second slices, respectively. Figure 5(f) shows the difference between phases in the second slice with and without the sample. The contrast represents the phase shift due to the upstream sample. It was found that even if the depth of focus is much longer than the sample thickness, i.e., the shape of the probe hardly changes within the sample, multislice ptychographic reconstruction works well. In the present experiment, the high-Q diffraction records information on fine structures of the illumination wave field on the second slice, which plays a key role in the multislice reconstruction.

In conclusion, we have demonstrated hard x-ray ptychography using a multislice approach in an experiment at

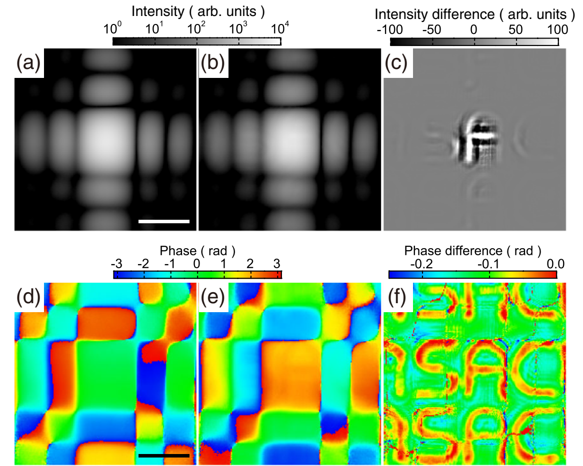

FIG. 5 (color online). Illumination wave field reconstructed using 3PIE. (a),(b) Intensity maps in the (a) first and (b) second slices. The scale bar is 1 μm. (c) Difference between the intensities in the second slice with and without the sample. (d),(e) Phase maps in the (d) first and (e) second slices. (f) Difference between the phases in the second slice with and without the sample. The illumination wave field in the second slice without the sample was derived using the angular spectrum method.

SPring-8. Ptychographic diffraction patterns of a two-layered object with a 105 μm gap were measured, and then the phase map of each layer was reconstructed at ~50 nm resolution beyond the limited spatial resolution under the projection approximation. To understand the convergence of the multislice reconstruction and the achievable spatial resolution, further experimental and theoretical investigations are desired. Additionally, it is crucial to generalize the multislice approach to unknown samples. In the present reconstruction using 3PIE, the gap width and the number of slices were treated as known parameters. Even if these parameters are unknown, optimum values can be determined through trial reconstructions; e.g., the condition minimizing the normalized error can be explored through 3PIE reconstructions with various gap widths and number of slices [32]. Furthermore, in the multislice approach for thick specimens without layered structures, increasing the number of slices will cause poor convergence in the phase retrieval calculation since the number of unknown variables will be much larger than the number of independent equations. To improve the convergence, the use of phase diversity should be effective [36]. For example, the illumination wave field can be diversified by the use of multiple x-ray energies and/or focused and defocused beams, which will increase the number of independent equations. At present, the spatial resolution in the beam propagation direction is much poorer than that in the transverse direction, which is mainly limited by the intensity of the incident x rays. The use of highly brilliant x-ray sources, such as an ultimate storage ring or an energy recovery linac, will enable us to improve the spatial resolution in the near future. Even for the limited

intensities of present synchrotron radiation facilities, high-resolution 3D observation should be realized by tomographic multislice phasing of the diffraction data recorded at various incident angles. We believe that multislice x-ray ptychography has the potential to enable the reconstruction of unknown objects and will open up a new frontier in the high-resolution 3D observation of extended thick specimens in materials science and biology.

This work was supported by a Grant-in-Aid for Young Scientists (A) (Grant No. 25709057) and JSPS Fellows (Grant No. 25.2959), and by the X-ray Free Electron Laser Priority Strategy Program from the Ministry of Education, Culture, Sports, Science and Technology.

*To whom all correspondence should be addressed.
takahashi@prec.eng.osaka-u.ac.jp

[1] R. Hegerl and W. Hoppe, Ber. Bunsen-Ges. Phys. Chem. **74**, 1148 (1970).
[2] J. M. Rondenburg, A. C. Hurst, and A. G. Cullis, Ultramicroscopy **107**, 227 (2007).
[3] H. N. Chapman and K. A. Nugent, Nat. Photonics **4**, 833 (2010).
[4] J. Miao, P. Charalambous, J. Kirz, and D. Sayre, Nature (London) **400**, 342 (1999).
[5] J. M. Rodenburg, A. C. Hurst, A. G. Cullis, B. R. Dobson, F. Pfeiffer, O. Bunk, C. David, K. Jefimovs, and I. Johnson, Phys. Rev. Lett. **98**, 034801 (2007).
[6] K. Giewekemeyer, P. Thibault, S. Kalbfleisch, A. Beerlink, C. M. Kewish, M. Dierolf, F. Pfeiffer, and T. Salditt, Proc. Natl. Acad. Sci. U.S.A. **107**, 529 (2010).
[7] M. Dierolf, A. Menzel, P. Thibault, P. Schneider, C. M. Kewish, R. Wepf, O. Bunk, and F. Pfeiffer, Nature (London) **467**, 436 (2010).
[8] P. Godard, G. Carbone, M. Allain, F. Mastropietro, G. Chen, L. Capello, A. Diaz, T. H. Metzger, J. Stangl, and V. Chamard, Nat. Commun. **2**, 568 (2011).
[9] S. O. Hruszkewycz , M. V. Holt, C. E. Murray, J. Bruley, J. Holt, A. Tripathi, O. G. Shpyrko, I. McNulty, M. J. Highland, and P. H. Fuoss, Nano Lett. **12**, 5148 (2012).
[10] Y. Takahashi, A. Suzuki, S. Furutaku, K. Yamauchi, Y. Kohmura, and T. Ishikawa, Phys. Rev. B **87**, 121201(R) (2013).
[11] A. Tripathi, J. Mohanty, S. H. Dietze, O. G. Shpyrko, E. Shipton, E. E. Fullerton, S. S. Kim, and I. McNulty, Proc. Natl. Acad. Sci. U.S.A. **108**, 13393 (2011).
[12] S. O. Hruszkewycz, M. J. Highland, M. V. Holt, D. Kim, C. M. Folkman, C. Thompson, A. Tripathi, G. B. Stephenson, S. Hong, and P. H. Fuoss, Phys. Rev. Lett. **110**, 177601 (2013).
[13] Y. Takahashi, A. Suzuki, S. Furutaku, K. Yamauchi, Y. Kohmura, and T. Ishikawa, Appl. Phys. Lett. **102**, 094102 (2013).
[14] M. Beckers, T. Senkbeil, T. Gorniak, M. Reese, K. Giewekemeyer, S.-C. Gleber, T. Salditt, and A. Rosenhahn, Phys. Rev. Lett. **107**, 208101 (2011).
[15] A. M. Maiden, G. R. Morrison, B. Kaulich, A. Gianoncelli, and J. M. Rodenburg, Nat. Commun. **4**, 1669 (2013).
[16] P. Thibault, M. Dierolf, A. Menzel, O. Bunk, C. David, and F. Pfeiffer, Science **321**, 379 (2008).
[17] C. M. Kewish, M. G. Sicairos, C. Liu, J. Qian, B. Shi, C. Benson, A. M. Khounsary, J. V. Comamala, O. Bunk, J. R. Fienup, A. T. Macrander, and L. Assoufid, Opt. Express **18**, 23420(2010).
[18] A. Schropp, P. Boye, J. M. Feldkamp, R. Hoppe, J. Patommel, D. Samberg, S. Stephan, K. Giewekemeyer, R. N. Wilke, T. Salditt, J. Gulden, A. P. Mancuso, I. A. Vartanyants, E. Weckert, S. Schöder, M. Burghammer, and C. G. Schroer, Appl. Phys. Lett. **96**, 091102 (2010).
[19] A. Schropp, R. Hoppe, V. Meier, J. Patommel, F. Seiboth, H. J. Lee, B. Nagler, E. C. Galtier, B. Arnold, U. Zastrau, J. B. Hastings, D. Nilsson, F. Uhlén, U. Vogt, H. M. Hertz, and C. G. Schroer, Sci. Rep. **3**, 1633 (2013).
[20] P. Thibault and A Menzel, Nature (London) **494**, 68 (2013).
[21] Y. Takahashi, A. Suzuki, N. Zettsu, Y. Kohmura, Y. Senba, H. Ohashi, K. Yamauchi, and T. Ishikawa, Phys. Rev. B **83**, 214109 (2011).
[22] A. Schropp, R. Hoppe, J. Patommel, D. Samberg, F. Seiboth, S. Stephan, G. Wellenreuther, G. Falkenberg, and C. G. Schroer, Appl. Phys. Lett. **100**, 253112 (2012).
[23] J. V. Comamala, A. Diaz, M. G. Sicairos, A. Mantion, C. M. Kewish, A. Menzel, O. Bunk, and C. David, Opt. Express **19**, 21333 (2011).
[24] K. Nugent, Adv. Phys. **59**, 1 (2010).
[25] H. N. Chapman, A. Barty, S. Marchesini, A. Noy, S. P. Hau-Riege, C. Cui, M. R. Howells, R. Rosen, H. He, J. C. H. Spence, U. Weierstall, T. Beetz, C. Jacobsen, and D. Shapiro, J. Opt. Soc. Am. A **23**, 1179 (2006).
[26] Y. Takahashi, Y. Nishino, R. Tsutsumi, N. Zettsu, E. Matsubara, K. Yamauchi, and T. Ishikawa, Phys. Rev. B **82**, 214102 (2010).
[27] K. S. Raines, S. Salha, R. L. Sandberg, H. Jiang, J. A. Rodríguez, B. P. Fahimian, H. C. Kapteyn, J. Du, and J. Miao, Nature (London) **463**, 214 (2010).
[28] J. M. Cowley and A. F. Moddie, Acta Crystallogr. **10**, 609 (1957).
[29] A. M. Maiden, M. J. Humphry, and J. M. Rondenburg, J. Opt. Soc. Am. A **29**, 1606 (2012).
[30] C. T. Putkunz, M. A. Pfeifer, A. G. Peele, G. J. Williams, H. M. Quiney, B. Abbey, K. A. Nugent, and I. McNulty, Opt. Express **18**, 11746 (2010).
[31] K. Tamasaku, Y. Tanaka, M. Yabashi, H. Yamazaki, N. Kawamura, M. Suzuki, and T. Ishikawa, Nucl. Instrum. Methods Phys. Res., Sect. A **467–468**, 686 (2001).
[32] See Supplemental Material at http://link.aps.org/supplemental/10.1103/PhysRevLett.112.053903 for derivation of equations of thickness criterion in CDI and spatial resolution in multislice x-ray ptychography, and convergence of multislice reconstruction by 3PIE.
[33] A. M. Maiden and J. M. Rodenburg, Ultramicroscopy **109**, 1256 (2009).
[34] M. Dierolf, P. Thibault, A. Menzel, C. M. Kewish, K. Jefimovs, I. Schlichting, K. König, O. Bunk, and F. Pfeiffer, New J. Phys. **12**, 035017 (2010).
[35] J. W. Goodman, *Introduction to Fourier Optics* (McGraw-Hill, New York, 1996), 2nd. ed., Chap. 3.
[36] C. T. Putkunz, J. N. Clark, D. J. Vine, G. J. Williams, M. A. Pfeifer, E. Balaur, I. McNulty, K. A. Nugent, and A. G. Peele, Phys. Rev. Lett. **106**, 013903 (2011).